In situ direct observation of photocorrosion in ZnO crystals in ionic liquid using a laser-equipped high-voltage electron microscope

J. Ishioka, K. Kogure, K. Ofuji, K. Kawaguchi, M. Jeem, T. Kato, T. Shibayama, and S. Watanabe

Citation: AIP Advances **7**, 035220 (2017); doi: 10.1063/1.4979726
View online: http://dx.doi.org/10.1063/1.4979726
View Table of Contents: http://aip.scitation.org/toc/adv/7/3
Published by the American Institute of Physics

In situ direct observation of photocorrosion in ZnO crystals in ionic liquid using a laser-equipped high-voltage electron microscope

J. Ishioka,[1,a] K. Kogure,[2] K. Ofuji,[2] K. Kawaguchi,[2] M. Jeem,[2] T. Kato,[1,3] T. Shibayama,[1,b] and S. Watanabe[1,c]
[1]*Centre for Advanced Research of Energy and Materials Faculty of Engineering, Hokkaido University, N13, W8, Kita-ku, Sapporo, Hokkaido 060-8628, Japan*
[2]*Graduate School of Engineering, Hokkaido University, N13, W8, Kita-ku, Sapporo, Hokkaido 060-8628, Japan*
[3]*Marketing and Sales Unit, Analysis, Testing and Research Business, Kobelco Research Institute, Inc., 1-11-2 Osaki, Shinagawa-ku, Tokyo 141-0032, Japan*

(Received 12 January 2017; accepted 23 March 2017; published online 30 March 2017)

ZnO photocatalysts in water react with environmental water molecules and corrode under illumination. ZnO nanorods in water can also grow because of water splitting induced by UV irradiation. To investigate their morphological behavior caused by crystal growth and corrosion, here we developed a new laser-equipped high-voltage electron microscope and observed crystal ZnO nanorods immersed in ionic liquid. Exposing the specimen holder to a laser with a wavelength of 325 nm, we observed the photocorrosion *in situ* at the atomic scale for the first time. This experiment revealed that Zn and O atoms near the interface between the ZnO nanorods and the ionic liquid tended to dissolve into the liquid. The polarity and facet of the nanorods were strongly related to photocorrosion and crystal growth. [http://dx.doi.org/10.1063/1.4979726]

By combining transmission electron microscopy (TEM) and various specimen-fabrication techniques, researchers recently achieved *in situ/operando* observation at high spatial resolution.[1–15] In general, specimen evaporation during TEM often causes critical damage to the electron gun and specimen chamber, so researchers have tried to seal such specimens in holders made from membranes of silicon nitride or SiO_2.[1–6] By accelerating electrons through such sets of thin membranes, researchers have managed to observe specimens in solution. In the other research, researchers have observed materials in an ionic liquid medium, which is stable and nonevaporative in ultrahigh vacuum.[7–12] However, most of those techniques must be modified for use in conventional TEM operating at 200 kV. To investigate the behavior of a specimen in liquid at high resolution, it is important to use a thinner membrane. Graphene is a promising thin film for sealing or channeling liquid around a specimen.[13–15] On the other hand, high-voltage electron microscopy (HVEM) is advantageous due to the transparency of its electron beam in order to eliminate the limitation of the maximum thickness of such a film. Although in situ HVEM observation is a promising way to examine specimens on the nanometer-to-micrometer scale while maintaining high resolution, there is little work on observing chemical reactions in liquid while applying electric fields, photon beam irradiation, or ion irradiation. These techniques will enable observation of nanoscale processes at greater detail, aiding the development of functional materials.

In this study, we produced a liquid environment in which crystals irradiated with visible light could be observed at atomic resolution. To allow for a sufficient volume of liquid to assist the chemical reaction while using a conventional microscopy method with high resolution, we combined

[a]Electronic mail: ishioka@eng.hokudai.ac.jp.
[b]Electronic mail: shiba@qe.eng.hokudai.ac.jp.
[c]Electronic mail: sw004@eng.hokudai.ac.jp.

HVEM with a laser irradiation system[16–18] inside a TEM chamber (Fig. 1). We name this microscope the multi-quantum-beam HVEM (MQB-HVEM). To confirm the effect of irradiation, we studied crystalline ZnO nanorods grown in water under UV irradiation.[19,20] These crystals are known to be self-corrosive under submerged illumination. Rather than water, we used ionic liquid for a safe fluid environment. Using the MQB-HVEM, we studied the photocorrosion of the ZnO nanorods at atomic resolution, confirming that an ionic liquid is a suitable medium in which to observe photochemical reactions by using *in situ* TEM.

Figure 1(a) shows a picture of the MQB-HVEM equipment (JEM-ARM-1300, JEOL, Japan). We have used ion-beam irradiation and *in situ* TEM in previous work.[21,22] In the present study, we added an optical path to directly irradiate the specimen by sharing part of the ion-beam line (Fig. 1(b)). The maximum total output of the 325-nm continuous-wave laser was roughly 8–16 mW. The laser was focused to a diameter of 0.5–1 mm on the TEM specimen. Using a charge-coupled device (CCD) camera installed under the camera chamber, we obtained a video constructed from TEM images with a maximum frame rate of 30 frames per second. Using these systems, we controlled the laser intensity and observed the specimen at the point irradiated by the laser.

Recently, Jeem *et al.* discovered a way to produce metal-oxide nanocrystals in ultrapure water via submerged photosynthesis of crystallites (SPSC),[19,20] which built wurtzite ZnO nanorods from

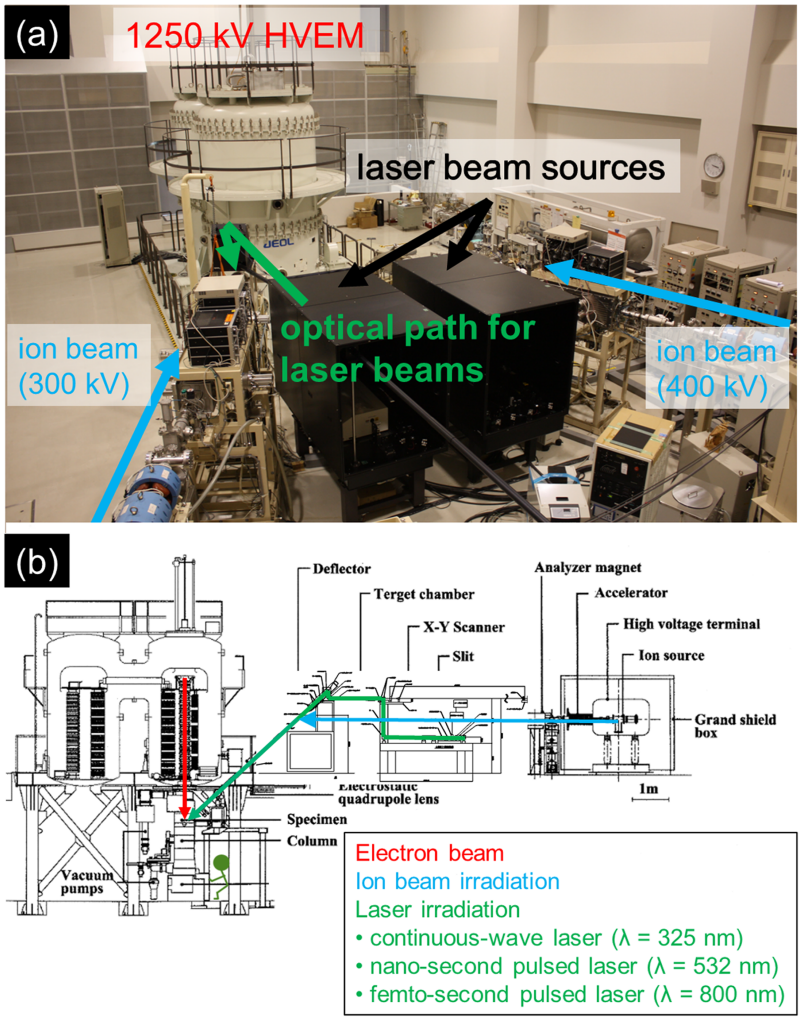

FIG. 1. Multi-quantum-beam high-voltage electron microscope (MQB-HVEM). (a) A photo of the upper half of the MQB-HVEM, including the electron accelerator, ion-beam lines, and optical systems, for which three laser sources can be selected. (b) A cross-sectional schematic of the MQB-HVEM, showing the three beam lines.

Zn^{2+} ions dissolved in water and from O^{2-} ions produced by the photocatalytic effect of H_2O under UV irradiation. This synthesis process requires no additives, unlike other methods.[23–28]

Figure 2 shows scanning electron microscopy (SEM) images that show the process of generating a crystal seed on the Zn substrate, which was treated by submerged plasma discharge,[29,30] ZnO crystal growth by UV irradiation, and photocorrosion in excess UV irradiation in fresh, pure water. As shown in Fig. 2(a), the plasma-treated Zn surface had ZnO nanobumps with a typical diameter of 10–20 nm, which later acted as nucleation centers for ZnO nanorods.[19] The Zn substrate in ultrapure water was irradiated *ex situ* using a UV lamp (UVP, B-100AP, USA) with 100-W long-wave UV (λ = 365 nm, 3.4 eV). After irradiation for 72 h, the crystal growth toward the *c*-axis had almost completed, and many ZnO nanocrystals had formed nanoflowers (Fig. 2(b)). This process is expected to include two simultaneous processes: apical growth at the crystal tips, and photocorrosion at the root of the crystal or Zn substrate. Once the Zn plate with ZnO crystals was placed in another cell of ultra-pure water and irradiated again by UV light, the final surface of the ZnO corroded and further crystal growth began (Fig. 2(c)). This process does not need any catalytic metals such as Pt; the polarized ZnO crystal structure itself enables the water splitting. Thus, to produce highly efficient crystal growth, we must control the properties of the water, which we are now investigating. However, because of the photocatalytic properties of ZnO, photocorrosion caused by illumination remains an issue. To make ZnO suitable for this application such as water splitting and gas production, its photocorrosion and crystal growth must be controlled. However, we have not yet observed its photocorrosion process *in situ* at the atomic scale with a microscope.

To observe the photochemical reaction by using TEM, we placed a TEM grid with thin amorphous carbon films on a Mo metal frame (Quantifoil, 200 mesh, R1.2/1.3, Großlöbichau, Germany) in a water

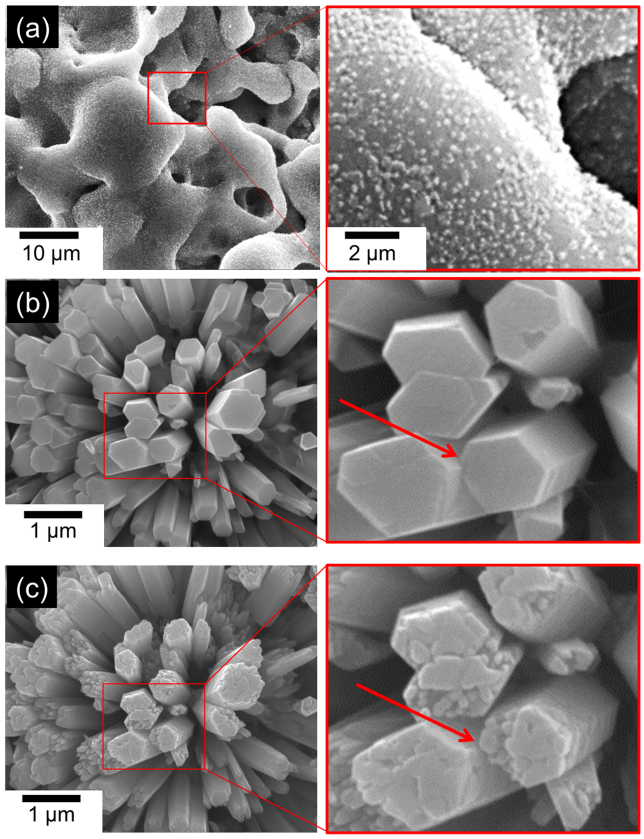

FIG. 2. Seeding, growth, and photocorrosion of ZnO nanocrystals. (a) Scanning electron microscopy (SEM) images of the plasma-treated Zn substrate, showing many nanoparticles embedded in its molten surface. (b) SEM images of typical ZnO nanoflowers, which were grown in ultrapure water irradiated by UV (λ = 365 nm) light for 72 h. (c) SEM images of corroded ZnO nanoflowers, which were UV-irradiated in fresh, ultrapure water by the same experimental setup.

cell together with the plasma-treated Zn substrate. Figure 3(a) shows the experimental setup used for UV irradiation. The water cell including the Zn plate was tilted, and the underside of the cell was irradiated by UV light. During UV irradiation, some of the generated pencil-like nanorods experienced photocorrosion and dropped onto the TEM grid. These nanorods on the TEM grid then regrew or corroded. After the ZnO nanorods had been deposited on the TEM grid, they were typically pencil-like single crystals and twinned structures. Figure 3(b) shows a typical twin-structured nanocrystal and a diffraction image in the $[1\bar{1}0]$ incident direction, obtained from the circled areas. The samples were observed by using conventional 200 kV field-emission TEM before immersion in ionic liquid. To characterize the crystals' polarity, we assessed their convergent-beam electron-diffraction patterns. The diffraction pattern taken from the tip of crystal was consistent with the calculated image for a 50-nm-thick crystal (Fig. 3(d)). Along the crystals, there was an oxygen-rich surface near the tip (Fig. 3(e)), which indicates that the tiny nanocrystals that had dropped from the original Zn substrate became nucleation centers for nanocrystals and wurtzite crystals to grow in the water. Overall, in this system, these ZnO nanocrystals grew more than they corroded.

To make a fluid environment around the ZnO crystals, we used the ionic liquid N,N,N-trimethyl-N-propylammonium bis(trifluoromethanesulfonyl)imide (TMPA-TFSI), which has a vapor pressure much lower than that of the TEM specimen chamber, and has an electronic conductivity sufficient to avoid charging the specimen. By dropping TMPA-TFSI onto the TEM grid with the ZnO nanocrystals and removing excess liquid,[8] we produced an inexpensive liquid cell that allowed for easy TEM. To produce high-resolution *in situ* TEM images, we searched the area filled with ionic liquid in the

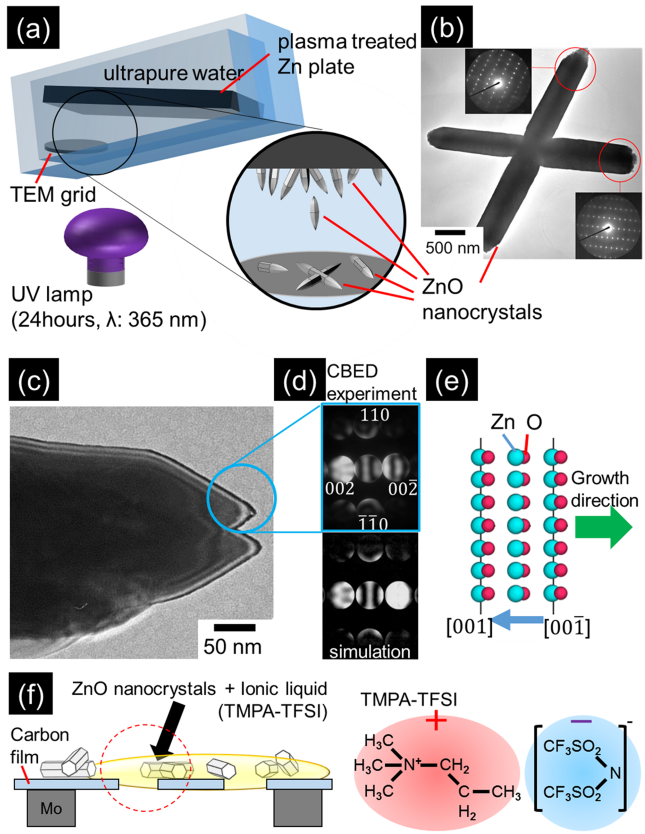

FIG. 3. Sample preparation via submerged photosynthesis of crystallites (SPSC),[19] and characterization of generated ZnO crystals by using 200 kV transmitted electron microscopy (TEM). (a) Schematic of ZnO crystal deposition and regrowth on a TEM grid. (b) TEM image of a ZnO nanocrystal with a twin structure along $[1\bar{1}0]$. (c) TEM image of the tip of a ZnO crystal with a pencil-like shape. (d) Convergent-beam electron diffraction (CBED) pattern obtained from the edge of the crystal shown in (c) and a numerically simulated pattern for a crystal with a thickness of 50 nm. (e) Atomic arrangement near a crystal tip, derived from CBED patterns. (f) Schematic of the observable area of ZnO crystals covered with TMPA-TFSI ionic liquid on a thin holey carbon film.

carbon holes holding ZnO nanocrystals (Fig. 3(f)), and then we exposed the area to continuous-wave laser irradiation.

Figure 4 shows the photocorrosion induced by laser irradiation for 90 min. In advance, we observed the ZnO tip immersed in TMPA-TFSI for 30 min at an electron intensity of 2 A/cm^2, revealing no change in the crystal structure or interfacial liquid (Fig. 4(b)). Here, we maintained the resolution during laser irradiation (Fig. 4(c)–(d)). Thirty minutes after irradiation, the crystal surface near the TMPA-TFSI appeared to change. When we slightly defocused the electron beam during irradiation, void-like structures clearly appeared across the entire ZnO surface. After 90 min (Fig. 4(d)), the crystal tip indicated by the red arrow had completely disappeared. To show the morphological change in the crystal tip, we captured a TEM image with large defocus. After finishing the laser irradiation, we observed the ZnO crystal with electrons again for about 30 min, confirming that the electron irradiation alone did not further change the crystal structure.

Figure 4(e) shows the change in ZnO morphology near the observed area. We obtained a visible outline as a reference from the images before irradiation and then obtained the reduction of the scale at the edges of the outline, indicated in Fig. 4(e) as points A–E. At point A, a concave edge, there were few changes in shape after irradiation (0.3 nm). However, at points B, D, and E in the convex edge, which were mainly terminated by oxygen atoms, the sizes decreased significantly: by 1.0 nm, 1.1 nm, and 0.8 nm, respectively. At point C, the edge also corroded by 0.5 nm along the [001] direction of ZnO. Because B–C is a {002} facet, these results clearly demonstrate faceted photocorrosion caused by polarity. The sides of the crystals were relatively stable. The crystal surface morphology did not

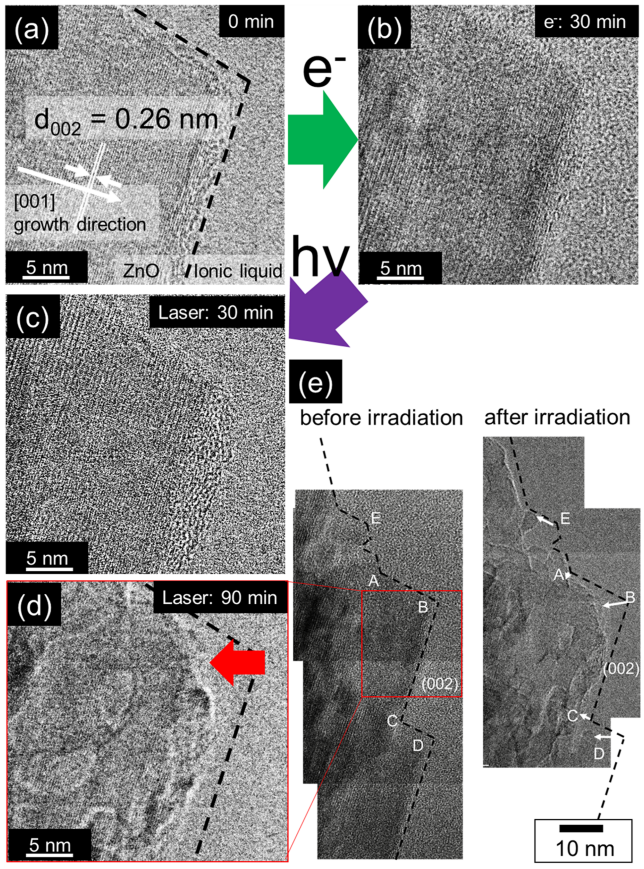

FIG. 4. *In situ* high-resolution TEM images showing the fabricated ZnO specimen in TMPA-TFSI ionic liquid, revealing photocorrosion at the atomic scale. (a), (b) High-resolution image from the [1$\bar{1}$0] axis at the tip of a ZnO nanorod irradiated by an electron beam at 2 A/cm^2 for (a) 0 min and (b) 30 min. (c), (d) High-resolution image of the tip of a ZnO nanorod irradiated by an electron beam at 2 A/cm^2 and by a 325-nm continuous-wave laser for (c) 30 min and (d) 90 min. (e) TEM images of a ZnO tip before and after irradiation. The broken line indicates the initial shape of the ZnO crystal, dividing the image into ZnO (with lattice fringes along the [001] direction) and TMPA-TFSI (with an amorphous pattern).

change in places with no ionic liquid. Thus, in the ionic liquid, ZnO crystals exposed to 325-nm laser irradiation tended to corrode rather than grow, especially at the crystal tip, which is weaker than other surfaces. These results show that corrosion in this system is strongly related to the crystal morphology and physical properties of the surface. To confirm the effect of laser irradiation, we performed another two experiments: using only laser irradiation in HVEM chamber and using *ex situ* irradiation in atmosphere for an extremely long time. These results (Figs. S1, S2 in the supplemental materials) show that laser irradiation was essential to causing photocorrosion.

To consider the mechanism of photocorrosion, we expect interband excitation by photons with an energy of 3.8 eV corresponding to the 325-nm laser, which delivers enough energy to excite electrons from the valence band of typical ZnO crystals with a band-gap energy of 3.37 eV. The incident light-excited electrons then generated holes near the surface. As noted by Jeem *et al.*,[19] when there is water near the surface, holes react with H_2O molecules to make OH radicals and H^+ ions. Jeem *et al.*[19] proposed the following whole chemical reactions:

$$\mathrm{ZnO} + \mathrm{h}\nu \rightarrow \mathrm{ZnO}(e_{CB}{}^{-} + h_{VB}{}^{+}) \cdots \quad (1)$$

$$H_2\mathrm{O} + h_{VB}{}^{+} \rightarrow \cdot OH + H \cdots \quad (2)$$

$$\cdot\mathrm{OH} + e_{aq}{}^{-} \rightarrow OH^{-}\ [\text{via hydrated electron}\ e_{CB}{}^{-} \rightarrow e_{aq}{}^{-}] \cdots \quad (3)$$

$$\mathrm{Zn} + 2H_2\mathrm{O} \rightarrow Zn^{2+} + 2OH^{-} + H_2\,(\mathrm{g})\ [\text{metal dissolution}] \cdots \quad (4)$$

$$Zn^{2+} + 2OH^{-} \rightarrow ZnO + H_2O\ [\text{crystal growth}] \cdots \quad (5)$$

$$\mathrm{Zn} + H_2O + h\nu \rightarrow ZnO + H_2\,(g) \cdots NET.$$

However, because of the lack of water molecules near the ionic liquid and ZnO, ZnO presumably splits into Zn^+ ions and $1/2O_2$. Then, $[TFSI]^-$ ions trap dissolved Zn^+ ions. So far, we propose the mechanism of photocorrosion as follows:

$$\mathrm{ZnO} + \mathrm{h}\nu \rightarrow \mathrm{ZnO}(e_{CB}{}^{-} + h_{VB}{}^{+}) \cdots \quad (1)$$

$$\mathrm{ZnO} + 2h_{VB}{}^{+} \rightarrow Zn^{2+} + {}^{1}\!/_{2}O_2(\text{in solution}) \cdots \quad (6)$$

$$2e_{CB}{}^{-} + \mathrm{O} \rightarrow O^{2-} \cdots \quad (7)$$

$$\mathrm{ZnO} + \mathrm{h}\nu \rightarrow Zn^{2+} + O^{2-} \cdots NET.$$

A detailed analysis will be required in future studies.

The laser-equipped HVEM is an alternative way to observe photochemical reactions in liquid at atomic resolution. Currently, there are two promising approaches: employing a liquid flow cell as used in environmental TEM, and using ionic liquid. The liquid flow cell has developed rapidly, and many experiments have shown it to be a powerful research tool.[1–6] However, most of these cells were fabricated for use in conventional TEMs operating at 200–300 kV. When using an electron-focusing technique such as spherical aberration correction, the liquid thickness remains a concern because of enhancement of the specimen damage due to well-focused electron beam. Moreover, the gas volume inside the cell may increase from water radiolysis or from heating induced by the electron beam, and such gas may break the thin observation windows. Therefore, using TEM with a liquid flow cell still requires a highly skilled operator to avoid hardware troubles, because controlling the environment around the specimen in these delicate systems is relatively difficult compared to doing so in an HVEM.

Conversely, conventional sample preparation methods for using ionic liquid have spread developed among chemists and biologists because it prevents charging in insulating specimens and keeps the specimen wet,[7–12] which is often advantageous. Although hardening by electron irradiation is another problem, the ease of sample preparation and stability of the ionic liquid in vacuum makes this technique very valuable. However, an ionic liquid film that is too thin causes a rapid decrease

in fluidity around the specimen during electron or laser irradiation. To observe for long durations, a thicker liquid will be advantageous, though using one will decrease the image contrast taken by a 200-kV TEM.

Compared with these two approaches, our method has several advantages. Because of the large specimen chamber around the pole pieces, we can add another detector to study the sample conditions or properties. Moreover, in large chamber few gas generated from specimen does not influence the vacuum rapidly so that the system allows us to image "dirtier" specimens at high resolution. Thus, our approach is a fairly conventional option for researchers whose direct observation experiments have proved insufficient or who want to combine measurements of physical properties and *in situ* observations.

Recently, employing a femtosecond laser and the photoelectric effect, ultrafast reactions have been observed with TEM.[31] In contrast, we have developed TEM equipment that observes slower chemical reactions in stable conditions. Specimen drift can be reduced by using weak, continuous light and electrons, allowing us to take high-resolution TEM images easily and continuously. Although several methods for observing photodecomposition with conventional TEM have been reported,[32,33] the higher transparency of electrons in MQB-HVEM makes it a powerful tool for observing thicker specimens in liquid environments. We have also constructed nanosecond and femtosecond pulsed lasers, which can go in a common optical path in MQB-HVEM. This state-of-the-art equipment will broaden TEM research not only to equilibrium materials but also to non-equilibrium processes.

In conclusion, we observed the photocorrosion of semiconducting nanorods in liquid at atomic resolution by using a new microscopy technique. Our technique will help in observing a wide range of photochemical reactions in chemical synthesis, electrochemical reactions, and biological processes, providing an easy way to prepare samples while maintaining stable conditions in large TEM specimen chambers.

SUPPLEMENTARY MATERIAL

See supplementary material for the further experimental results of photocorrosion under laser irradiation.

ACKNOWLEDGMENTS

This study was supported by the "Nanotechnology Platform" Program of the Ministry of Education, Culture, Sports, Science and Technology (MEXT) of Japan (Grant Nos. HNPA 14–058 and HNPA 15–064), and the Japan Society for the Promotion of Science (JSPS) Grant-in-Aid for Young Scientists (C) #26870012. The authors thank Prof. N. Sakaguchi, Prof. S. Yatsu, Mr. K. Ohkubo, Mr. T. Tanioka, Mr. R. Oota, and Ms. N. Hirai for their technical assistance and helpful discussions.

[1] J. E. Evans, K. L. Jungjohann, N. D. Browning, and I. Arslan, "Controlled growth of nanoparticles from solution with *in situ* liquid transmission electron microscopy," Nano Lett. **11**(7), 2809 (2011).
[2] N. Jonge and F. M. Ross, "Electron microscopy of specimens in liquid," Nature Nanotech. **6**, 695 (2011).
[3] M. Gu, L. R. Parent, B. L. Mehdi, R. R. Unocic, M. T. McDowell, R. L. Sacci, W. Xu, J. G. Connell, P. Xu, P. Abellan, X. Chen, Y. Zhang, D. E. Perea, J. E. Evans, L. J. Lauhon, J. G. Zhang, J. Liu, N. D. Browning, Y. Cui, I. Arslan, and C.-M. Wang, "Demonstration of an electrochemical liquid cell for *operando* transmission electron microscopy observation of the lithiation/delithiation behavior of Si nanowire battery anodes," Nano Lett. **13**, 6106 (2013).
[4] T. J. Woehl, C. J. Park, E. Evans, I. Arslan, W. D. Ristenpart, and N. D. Browning, "Direct observation of aggregative nanoparticle growth: Kinetic modeling of the size distribution and growth rate," Nano Letters **14**, 373 (2013).
[5] D. Li, M. H. Nielsen, J. R. I. Lee, C. Frandsen, J. F. Banfield, and J. J. Yoreo, "Direction-specific interactions control crystal growth by oriented attachment," Science **336**, 1014 (2012).
[6] H. G. Liao, L. Cui, S. Whitelam, and H. Zheng, "Real-time imaging of Pt_3Fe nanorod growth in solution," Science **336**, 1011 (2012).
[7] S. Kuwabata, A. Kongkanand, D. Oyamatsu, and T. Torimoto, "Observation of ionic liquid by scanning electron microscope," Chem. Lett. **35**, 600 (2006).
[8] T. Uematsu, M. Baba, Y. Oshima, T. Tsuda, T. Torimoto, and S. Kuwabata, "Atomic resolution imaging of gold nanoparticle generation and growth in ionic liquids," J. Am. Chem. Soc. **136**(39), 13789 (2014).
[9] S. Suzuki, Y. Tomita, S. Kuwabata, and T. Torimoto, "Synthesis of alloy AuCu nanoparticles with the L10 structure in an ionic liquid using sputter deposition," Dalton Trans. **44**, 4186 (2015).
[10] S. Chen, K. Kobayashi, R. Kitaura, Y. Miyata, and H. Shinohara, "Direct HRTEM observation of ultrathin freestanding ionic liquid film on carbon nanotube grid," ACS Nano **5**(6), 4902 (2011).

[11] K. Yoshida, T. Nozaki, T. Hirayama, and N. Tanaka, "*In situ* high-resolution transmission electron microscopy of photocatalytic reactions by excited electrons in ionic liquid," Journal of Electron Microscopy **56**(5), 177–180 (2007).
[12] D. Sugioka, T. Kameyama, S. Kuwabata, and T. Torimoto, "Single-step preparation of two-dimensionally organized gold particles via ionic liquid/metal sputter deposition," Phys. Chem. Chem. Phys **17**, 13570 (2015).
[13] J. M. Yuk, J. Park, P. Ercius, K. Kim, D. J. Hellebusch, M. F. Crommie, J. Y. Lee, A. Zettl, and A. P. Alivisatos, "High-resolution EM of colloidal nanocrystal growth using graphene liquid cells," Science **336**, 61 (2012).
[14] X. Ye, M. R. Jones, L. B. Frechette, Q. Chen, A. S. Powers, P. Ercius, G. Dunn, G. M. Rotskoff, S. C. Nguyen, V. P. Adiga, A. Zettl, E. Rabani, P. L. Geissler, and A. P. Alivisatos, "Single-particle mapping of nonequilibrium nanocrystal transformations," Science **354**(6314), 874.
[15] B. Radha, A. Esfandiar, F. C. Wang, A. P. Rooney, K. Gopinadhan, A. Keerthi, A. Mishchenko, A. Janardanan, P. Blake, L. Fumagalli, M. Lozada-Hidalgo, S. Garaj, S. J. Haigh, I. V. Grigorieva, H. A. Wu, and A. K. Geim, "Molecular transport through capillaries made with atomic-scale precision," Nature **538**, 222 (2016).
[16] S. Watanabe, Y. Yoshida, S. Kayashima, S. Yatsu, M. Kawai, and T. Kato, "In situ observation of self-organizing nanodot formation under nanosecond-pulsed laser irradiation on Si surface," J. Appl. Phys. **108**, 103510 (2010).
[17] Z. Yang, N. Sakaguchi, S. Watanabe, and M. Kawai, "Dislocation loop formation and growth under in situ laser and/or electron irradiation," Sci. Rep. **1**, 190 (2011).
[18] Z. Yang, S. Watanabe, and T. Kato, "The irradiation effect of a simultaneous laser and electron dual-beam on void formation," Sci. Rep. **3**, 1201 (2012).
[19] M. Jeem, M. R. M. bin Julaihi, J. Ishioka, S. Yatsu, K. Okamoto, T. Shibayama, T. Iwasaki, T. Kato, and S. Watanabe, "A pathway of nanocrystallite fabrication by photo-assisted growth in pure water," Sci. Rep. **5**, 1129 (2015).
[20] M. Jeem, L. Zhang, J. Ishioka, T. Shibayama, T. Iwasaki, T. Kato, and S. Watanabe, "Tuning optoelectrical properties of ZnO nanorods with excitonic defects via submerged illumination," Nano Lett. **17**(3), 2088 (2017).
[21] R. Yu, T. Shibayama, X. Meng, S. Takayanagi, Y. Yoshida, S. Yatsu, and S. Watanabe, "Effects of nanosecond-pulsed laser irradiation on nanostructure formation on the surface of thin Au films on SiO_2 glass substrates," Applied Surface Science **289**, 274–280 (2014).
[22] X. Meng, T. Shibayama, R. Yu, S. Takayanagi, and S. Watanabe, "Ion irradiation synthesis of Ag–Au bimetallic nano-spheroids in SiO_2 glass substrate with tunable surface plasmon resonance frequency," Journal of Applied Physics **114**, 054308 (2013).
[23] J. Joo, B. Y. Chow, M. Prakash, E. S. Boyden, and J. M. Jacobson, "Face-selective electrostatic control of hydrothermal zinc oxide nanowire synthesis," Nature Materials **10**, 596 (2011).
[24] L. Shi, K. Bao, J. Cao, and Y. Qian, "Sunlight-assisted fabrication of a hierarchical ZnO nanorod array structure," Cryst. Eng. Comm. **11**, 2009–2014 (2009).
[25] F. Ahmed, S. Kumar, N. Arshi, M. S. Anwar, and R. Prakash, "Growth and characterization of ZnO nanorods by microwave-assisted route: Green chemistry approach," Adv. Mat. Lett. **2**(3), 183 (2001).
[26] K. S. Kim, H. Jeong, M. S. Jeong, and G. Y. Jung, "Polymer-templated hydrothermal growth of vertically aligned single-crystal ZnO nanorods and morphological transformations using structural polarity," Adv. Funct. Mater. **20**, 3055 (2010).
[27] L. Xu, Y. L. Hu, C. Pelligra, C. H. Chen, L. Jin, H. Huang, S. Sithambaram, M. Aindow, R. Joesten, and S. L. Suib, "ZnO with different morphologies synthesized by solvothermal methods for enhanced photocatalytic activity," Chem. Mater. **21**, 2875 (2009).
[28] Y. Ding, K. C. Prade, and Z. L. Wang, "*In situ* transmission electron microscopy observation of ZnO polar and non-polar surfaces structure evolution under electron beam irradiation," J. Appl. Phys. **119**, 015305 (2016).
[29] Y. Toriyabe, S. Watanabe, S. Yatsu, T. Shibayama, and T. Mizuno, "Controlled formation of metallic nanoballs during plasma electrolysis," Applied Physics Letters **91**, 041501 (2007).
[30] M. R. M. bin Julaihi, S. Yatsu, and S. Watanabe, "Synthesis of stainless steel nanoballs via submerged glow-discharge plasma and its photocatalytic performance in methylene blue decomposition," Journal of Experimental Nanoscience **10**, 12 (2015).
[31] A. H. Zewail, "4D ultrafast electron diffraction, crystallography, and microscopy," Annu. Rev. Phys. Chem. **57**, 65 (2006).
[32] K. Yoshida, J. Yamasaki, and N. Tanaka, "In situ high-resolution transmission electron microscopy observation of photodecomposition process of poly-hydrocarbons on catalytic TiO_2 films," Appl. Phys. Lett. **84**, 2542 (2004).
[33] F. Cavalca, A. B. Laursen, B. E. Kardynal, R. E. Dunin-Borkowski, S. Dahl, J. B. Wagner, and T. W. Hansen, "*In situ* transmission electron microscopy of light-induced photocatalytic reactions," Nanotechnology **23**, 075705 (2012).